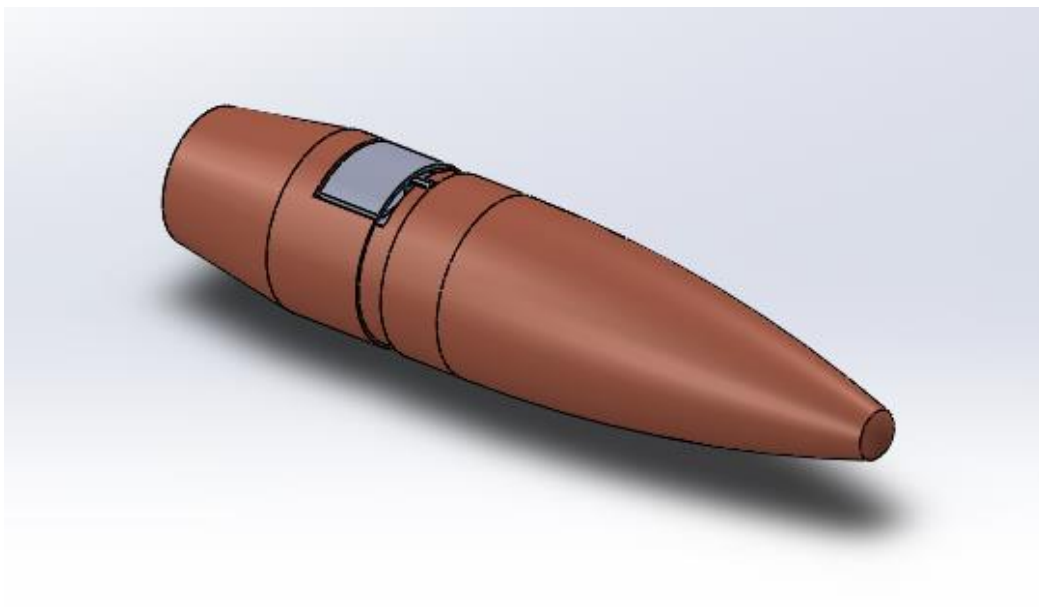# Design of a Smart Actuator
for
Small-Caliber Smart Munitions

Craig Chan, M.Eng. Aerospace Engineering '14
Ephrahim Garcia, Advisor

Master of Engineering 2013 – 2014 Report

Table of Contents

Table of Figures

Technical Report

Abstract

Smart munitions have the ability to control flight trajectory as they reach their targets. Although this is feasible for large munitions such as smart bombs and guided missiles, it is considerably more difficult for small-caliber munitions such as sniper rounds. Sniper rounds that can control flight trajectory have the potential to have benefits such as reducing civilian casualties in populated areas or hostage situations, rejecting disturbances such as wind, and decreasing bullet drop. These all reduce the calculations needed for a sniper to aim. Current research and control of small-caliber smart munitions, or smart bullets, require physically despinning the bullet. An approach for controlling the flight of bullets by allowing them to spin with a solid-state, high-frequency actuator to engage a control surface to modify its flight trajectory is possible. Both spoilers and Gurney flaps can be used to realize a "walking the precession" trajectory control. A smart actuator for spoiler deployment has been designed. The solid-state aspect is achieved using a piezoelectric stack, in which its small deflection can be mechanically amplified via a compliant structure. Using results from preliminary force predictions through CFD analysis, an actuated spoiler configuration and design requirements were determined. Design methods using ball and stick models for kinematic structures, comparing torsional stiffnesses, utilizing a dual amplification system for the compliant structure, and structural and piezoelectric FEA in ANSYS Workbench are discussed.

Nomenclature

f_{bl}	=	blocked force
δ_0	=	free displacement
d_{33}	=	piezoelectric strain coefficient along polarization direction
s_{33}^E	=	compliance of piezoelectric material along polarization direction under constant electric field
V_{stack}	=	applied voltage for piezoelectric stack
V_{bulk}	=	adjusted applied voltage for ANSYS piezoelectric bulk stack
t_p	=	individual piezoceramic plate thickness
L_3	=	length of piezoelectric stack actuator along polarization direction
A_s	=	piezoelectric stack cross-sectional area
ℓ	=	design link length for kinematic or compliant structure
θ	=	idle (initial) design angle for kinematic or compliant structure
θ'	=	engaged (final) design angle for kinematic or compliant structure
K	=	torsional stiffness
E	=	Young's modulus
I	=	area moment of inertia
l	=	length of flexure or more compliant link

Introduction

Controlling the flight trajectory of small-caliber munitions allows for tracking moving targets and rejecting disturbances such as wind. Smart bullets can have the potential of stabilizing flight and ensuring that only the HVT (High Value Target) is hit, reducing collateral damage. Snipers at long ranges of over 1.25 km may become more efficient when relying on such a technology. The rifling of barrels already allows for aerodynamic stability and accuracy through gyroscopic spin stabilization, but the bullet can always be subjected to disturbances or have a chance of missing a moving target. Kogan and Garcia proposed an actuation control scheme that does not require the munition to be physically despun. Their precession synchronized roll-based control (PSRBC) method controls the nutation and precession, both of which are slower than the spin rate of the bullet. This "walking the precession" allows the actuation bandwidth to be at the spin rate of the bullet rather than an order of magnitude higher if using roll-based control. They suggested that a control surface such as a spoiler or a Gurney flap engaged once per revolution can be used to control the flight trajectory without modifying the external geometry of a 0.50 caliber bullet. The spoiler or flap can cause an asymmetric drag on the bullet,

creating a moment about the bullet's center of gravity which then causes the bullet to rotate towards the desired direction.

Maintaining the small size of the 0.50 caliber bullet adds challenges to smart bullet design. Smart actuators, which utilize smart materials, can reduce the complexity of mechanical systems. Smart materials such as piezoelectric materials, shape memory alloys, or electroactive polymer materials exhibit coupling and convert energy between multiple physical domains. For the above materials, piezoelectric materials and electroactive polymer materials convert between the mechanical and electrical domains, while shape memory alloys convert between the thermal and mechanical domains. Since the bullet in question spins at 2.5 kHz, piezoelectric ceramics are used for the actuator design. Its response speed, stiffness, and stress output are among the highest of the known smart materials and therefore makes it the ideal candidate for this type of smart bullet. However, piezoelectric materials have a limited strain generation of approximately 0.1%. This small deflection can be mechanically amplified by acting against a compliant structure, resulting in a solid-state aspect that eliminates the need for moving parts such as hinges. The elastic properties of a compliant structure allows the actuator to return to the original disengaged state without expending more energy. This report discusses the design of an actuator engaging the spoiler for a 0.50 caliber BMG M33 round. Its dimensions are shown in Figure 1 with possible deployments shown in Figure 2.
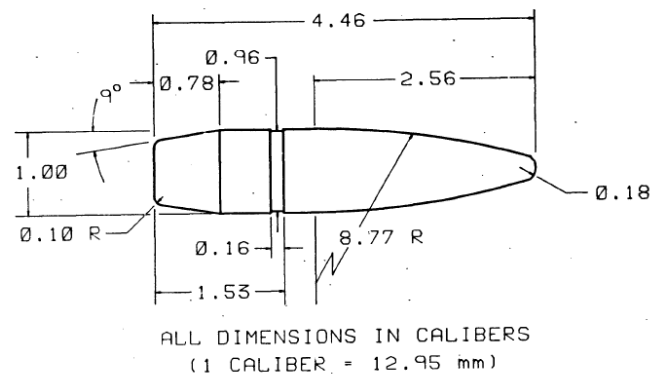

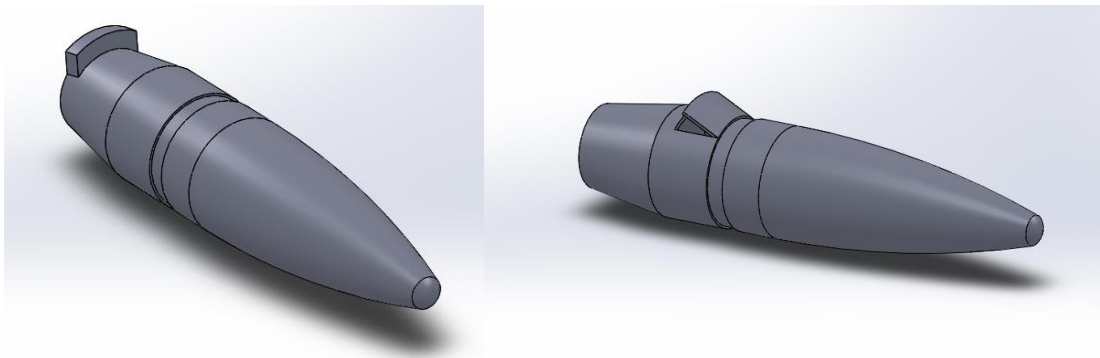**Figure 1: Dimensions for a 0.50 caliber M33 round [McCoy].**

Figure 2: Possible deployments for 0.50-caliber smart bullet. *Left: Gurney flap. Right: Spoiler.*

Preliminary Aerodynamic Analysis

Preliminary three-dimensional CFD simulations using ANSYS Fluent were done by Jonathan Mohr in the fall of 2013 to determine the potential aerodynamic forces acting on an engaged smart bullet traveling at Mach 2.653. he simulations assumed the bullet was non-spinning so that the results could be confirmed by wind tunnel testing. The results comparing the clean (unengaged) bullet and the engaged spoiler are shown in Table 1.

Table 1: Preliminary CFD Results

Configuration	Clean Bullet	Aerodynamic Spoiler (2 mm deployment)	Gurney Flap (2 mm deployment)
Drag Coefficient	0.354	0.370	0.377
Lift Coefficient	0.00300	-0.0688	-0.0631
Coefficient of Moment	9.52E-05	-7.91E-04	-7.83E-05
Total Drag (N)	23.262	27.184	25.890
Drag on Control Surface (N)	N/A	2.674	2.131
Total Lift (N)	0.198	-5.0586	-4.331
Total Moment (N·m)	0.00630	-0.0581	-0.00540

The deployment distance is defined as the perpendicular distance from the back edge of the spoiler to the surface of the bullet. For the Gurney flap, this is defined as the distance from the top of the flap to the bullet jacket surface. For a spoiler that is 5 mm long, this translates into a deflection angle of 23.6°. However, in this report, this will be referred to as the "2 mm deployment" requirement. Because of the greater moment induced by the spoiler, the design of a smart actuator exploring the deployment of a spoiler is explored in this report.

Piezoelectric Considerations

The two most important characteristics of a piezoelectric stack are the blocking force and the free displacement. The blocked force (Equation 1) is the force required for pushing back a fully energized piezoelectric actuator to zero displacement, and the free displacement (Equation 2) is the displacement achieved by an engaged actuator without working against any external load.

Equation 1
$$f_{bl} = \frac{d_{33}A_S V}{s_{33}^E t_p}$$

Equation 2
$$\delta_0 = \frac{d_{33}L_3}{t_p}V$$

Above, the intrinsic properties d_{33} and s_{33}^E are important design considerations. A higher d_{33} results in a higher piezoelectric stack strain at a given voltage, and a lower compliance (or a higher stiffness) results in a higher blocked force. These ultimately result in a greater deflection of the spoiler. For demonstration purposes of actuator design, a non-custom piezoelectric 5 mm x 5 mm x 36 mm P-885.91 piezoelectric stack actuator with PIC255 piezoceramic plates from Physik Instrumente (PI) was modeled in ANSYS Workbench. Although the stack can be modeled with its individual plates, it is easier and equivalent to model the stack as one solid rectangular block of the same piezoelectric material with adjusted voltage conditions. Equation 3 is used for this adjustment.

Equation 3
$$V_{bulk} = \frac{L_3 V_{stack}}{t_p}$$

It should be noted that for the P-885.91 stack actuator, the length was 36 mm and the thickness of the plates was 0.05 mm.

Table 2. P-885.91 (PIC255 material) piezoelectric stack ANSYS model results.

	ANSYS	Specifications	Percent error (%)
Blocked Force (N)	937	950	-1.4
Free Displacement (µm)	28	38	-26

The results in Table 2 show that the resulting design will be conservative. Of course, the material properties can be adjusted to better fit the specifications, but it was decided to keep the current numbers as they were given and remain conservative. In order to convert the small stack deflection into a 2 mm flap deflection, mechanical amplification must be used.

Compliant Structure Considerations and FEA

The mechanical amplification is achieved through a compliant structure. Figure 3 shows an example topology of the structure. The balls in the ball and stick model represent the compliant flexure hinges while the sticks represent the more rigid parts of the structure. The dotted rectangle represents the piezoelectric stack, and the direction of the free displacement is aligned with the negative or positive of the poling direction. This topology was chosen due to the sizes of the bullet and the piezoelectric stack actuator as well and the location of the spoiler on the bullet. The extension of the piezoelectric stack translates to an outward motion of the center links. The resulting mechanical amplification due to the bow-tie structure can be used to gain a lever-like mechanical advantage that will engage the spoiler.
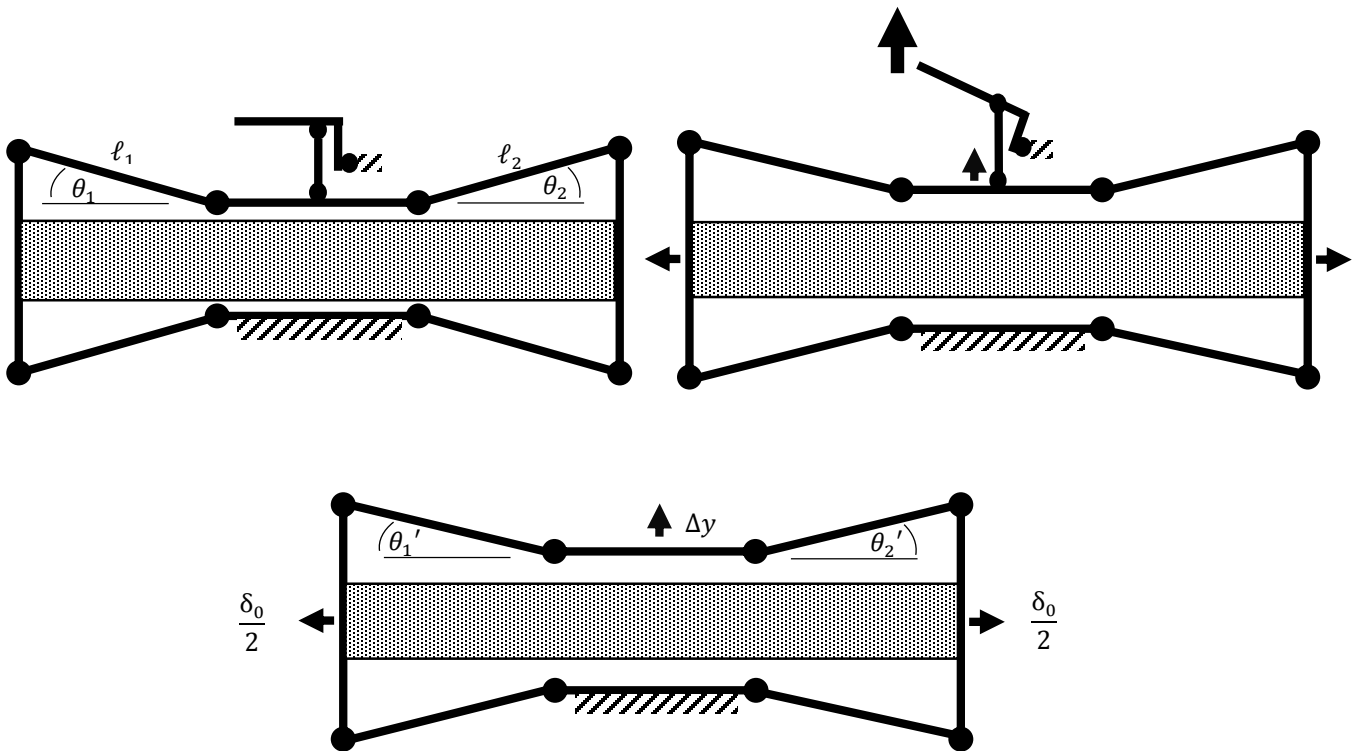

Figure 3: Compliant structure topology. *Left: Idle. Right: Engaged. Bottom: Engaged bow-tie alone.*

The engaged topology of a symmetric bow-tie structure ($l_1 = l_2 = l$ and $\theta_1 = \theta_2 = \theta$) can be found by idealizing it as a kinematic structure, shown in Figure 3. In a kinematic structure, the hinges are freely rotating links while the lines are completely rigid. The equations that describe the horizontal and vertical displacement of the model are

Equation 4
$$\frac{\delta_0}{2} = \ell(\sin \theta' - \sin \theta)$$

Equation 5
$$\Delta y = \ell(\cos \theta - \cos \theta')$$

For the kinematic structure, the horizontal displacement is assumed to be the free displacement. Solving for the vertical displacement after eliminating θ' by distributing, rearranging the terms, squaring the equations, and adding them together gives

Equation 6
$$\Delta y = \frac{1}{2}\sqrt{4\ell^2 \sin^2 \theta - \delta_0(4\,\ell \cos \theta + \delta_0)} + \ell \sin \theta$$

The amplification ratio is the output divided by the input, or

Equation 7
$$a = \frac{\Delta y}{\delta_0} = \frac{\frac{1}{2}\sqrt{4\ell^2 \sin^2 \theta - \delta_0(4\,\ell \cos \theta + \delta_0)} + \ell \sin \theta}{\delta_0}$$

It is important to note that the dimensions of the top and bottom center links have no effect on the output of the kinematic structure. However, for an actual compliant structure, the dimensions will affect the torsional stiffness of the bow-tie structure. Given the geometric constraints of the piezoelectric stack and the bullet, a desired length for the angled links can be chosen, and the optimal initial angle can be found (Equation 8).

Equation 8
$$\theta_{opt} = \cos^{-1}\frac{\delta_0}{4\ell}$$

For the μm scale of the free displacement and the mm scale of the angled links, θ_{opt} generally results in an angle that is slightly lower than 90°.

The model finally used for this project was an asymmetric bow-tie due to the geometric constraints of the bullet and desired placement of the lever arm. Through some experiments in ANSYS, asymmetric bow-ties were found to have marginally better outputs. The equations that describe the general asymmetric bow-tie structure are

Equation 9
$$\delta_0 = \ell_1(\sin \theta_1' - \sin \theta_1) + \ell_2(\sin \theta_2' - \sin \theta_2)$$

Equation 10
$$\Delta y = \ell_1(\cos \theta_1 - \cos \theta_1') = \ell_2(\cos \theta_2 - \cos \theta_2')$$

Equation 11
$$\theta_2 = \cos^{-1}\left(\frac{\ell_1}{\ell_2}\cos \theta_1\right)$$

Equation 12
$$\theta_2' = \cos^{-1}\left(\frac{\ell_1}{\ell_2}\cos \theta_1'\right)$$

The symbolic solution for the optimal design angle $\theta_{1,opt}$ is too long for this report or the Appendix and showing it will have no practical value, but it was also generally found to be slightly lower than 90° for the desired lengths. 89° was chosen for manufacturing reasons and to lower the chance of buckling. Theoretically, optimal lengths can be found, but this would only change the optimal angle. Therefore, only the optimal angle was needed. This characteristic was used in designing the actuator.

Traditional mechanical structures achieve compliance by connecting stiff parts to hinges, whereas compliant structures achieve this by using flexible parts. The flexible areas of the structure bend when a load is introduced. The flexibility of the configuration is affected by:

1. Material properties,
2. Geometry, and
3. Loading and boundary conditions.

Generally, a high strength to Young's modulus ratio is desired. A low Young's modulus results in greater deflections while a high strength ensures that the structure will not fail. The geometry of the structure is a main factor in deciding which parts are flexible and which parts are rigid. In most cases, it is desired for the flexible links to be much smaller in length and have cross-sections with smaller area moments of inertia in comparison to the more rigid links. The thinner the flexure is in one direction, the greater the deflection in that direction. However, the fatigue strength or the endurance limit is highly important when designing the smart bullet actuator as the high actuation bandwidths may result in fatigue failure. Therefore, spring steel was chosen for the material used to design the compliant mechanism. Although it has a nominal tensile yield strength of 1500 MPa, the nominal fatigue strength of 650 MPa was used as the limiting design criteria for the actuator. However, structural steel in ANSYS was used for modeling due to its readily available properties. Since the two have a very similar Young's modulus, this was deemed acceptable. The area moment of inertia of the flexure hinges were designed to be small enough to allow greater deflections but not exceed the fatigue strength, confirmed through finite element analysis (FEA).

Torsional stiffnesses of the flexures and the more rigid links were adjusted to help give the desired effect by adjusting the lengths. The stiffnesses were crucial design parameters to consider for the lower, bow-tie amplification system and the upper lever-arm-based amplification system. Equation 13 below was used to make design decisions.

Equation 13 $$K = \frac{EI}{l}$$

The bow-tie structure was considered the primary amplification system as it directly translated the piezoelectric actuator's displacement into an amplified output in a different direction, while the upper amplification system translated the bow-tie structure's output into the spoiler displacement. In order to counteract the opposing forces from the upper amplification system, the torsional stiffnesses throughout the bow-tie structure had to be greater than that of the amplification structure. This is why in the current design the length of the flexures are small (so more rigid links are needed) in the bow-tie structure while the compliant links in the upper amplification system are much longer. Also, because of the large deflections required for in the upper amplification system, I was small while l was large to reduce stress concentrations that could lead to plastic deformation or early fatigue failure. Figure 4 shows an example flexure with the above variables. Small-length flexural pivots were used in the design of the bow-tie structure.
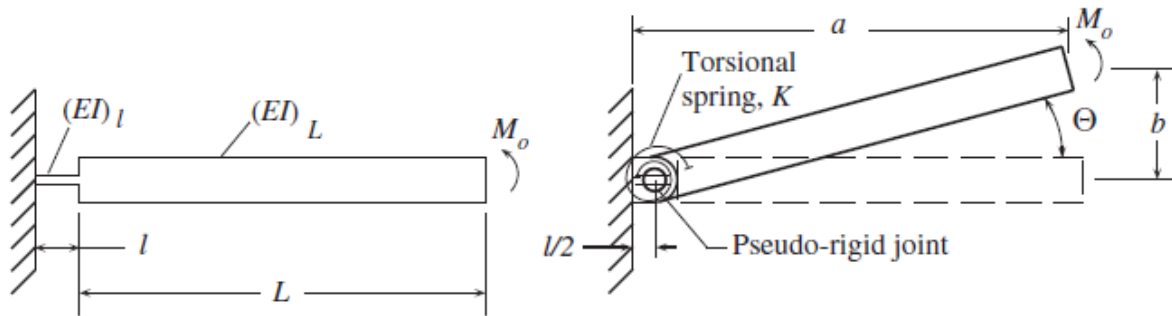

Figure 4: Pseudo-rigid-body model of a small-length flexural pivot [Howell, Magleby, Olsen].

To verify the above design considerations, the optimization tool in ANSYS was used to generate multiple experiments for the overall compliant structure. Although the structure was too complex to do full optimization in a timely fashion, the results were used to make design choices.

Even after utilizing the design methods above, there are numerous possibilities for the loading and boundary conditions of the flexure-based compliant mechanism. The structure exhibits different behavior depending on which portions are more compliant. Using finite element software such as ANSYS can simplify the design process by focusing on the important parts of the structure. As the actuator is designed to be part of the bullet structure instead of a separate component, simulation time can be saved by isolating the actuator and taking

the other, more rigid sections of the bullet structure into account by applying the appropriate boundary conditions (shown later).

Preliminary FEA in ANSYS Workbench with a piezoelectric extension showed that the above structure without the lever arm at 20 V applied to the piezoelectric bulk stack had a vertical displacement of 0.25 mm with total average horizontal placement of 13.1 μm, or an amplification ratio of 19.1. 120 V was not used as the structure would have a chance to buckle (120 V would result in a fully engaged bow-tie structure, i.e. a rectangle) after disengaging the piezoelectric actuator. A simple geometry calculation with a kinematic structure assumption showed that the required spoiler deployment would have been feasible. However, when the lever arm, hinge arm, spoiler, and loads due to the aforementioned CFD results were added, the current design did not meet its spoiler deployment criteria. Currently, there is a 1.24 mm deployment with a maximum von-Mises stress of 485 MPa at a voltage of 24.31 V. This means that with the input of 0.295 mm by the bow-tie structure, the upper amplification system alone had an amplification ratio of 4.2, and the total amplification ratio of the entire compliant structure with a total displacement of the piezoelectric actuator at 25 μm was 496. The increased voltage in this case was acceptable since the other parts of the compliant structure helped prevent the bow-tie from reaching maximum deployment, which again could result in buckling. Although this exceeds the fatigue strength, given the short lifetime of the bullet during flight, estimated to be about 1-2 sec, this is acceptable as it does not undergo plastic deformation. Quasi-static FEA using structural steel for the compliant structure (as spring steel fatigue data was not readily available) resulted in a strain lifetime of 9902 cycles, or 3.96 sec lifetime if constantly actuated at 2.5 kHz. This lifetime was found for ANSYS demonstration purposes, but since the fatigue strength for spring steel can be 650 MPa as stated above, it is possible that the current design has infinite life. Higher flap deployments may be reached at higher voltages, but it was observed that increasing the voltage would result in a much shorter life for the compliant structure and increase the chances for the bow-tie structure to buckle. Using actual spring steel with full elastic properties as intended, including fatigue, may result in a higher lifetime. Figure 5 show the idle and engaged compliant structure with the boundary conditions used to model the rest of the more rigid bullet structure. The results are summarized in Table 3.
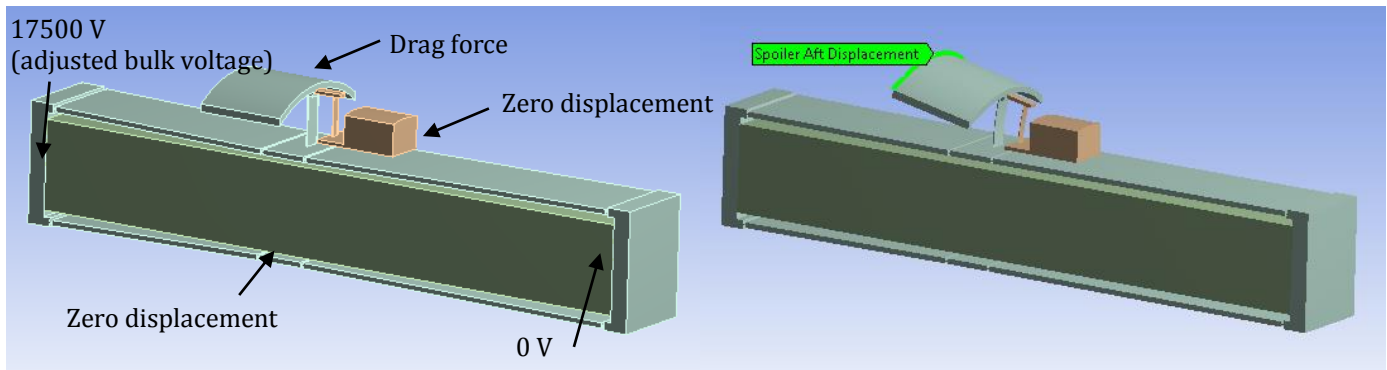

Figure 5: Piezoelectric stack actuator with compliant structure. *Left: Idle. Right: Engaged.*

Table 3: Summary of important results at 24.31 V.

Spoiler End Vertical Displacement	Maximum von-Mises Stress	Cycles to Fatigue Failure (Structural steel)	Cycles to Fatigue Failure (Spring steel)
1.24 mm	485 MPa	9902 cycles	Infinite (theoretically)

It is possible that if the compliant structure's natural frequencies were turned to the actuation bandwidth, a greater displacement may be achieved. However, this is beyond the scope of this project and report. To better visualize the rest of the bullet structure simulated using boundary conditions, Figure 6 shows a potential cross-section and exploded view of the smart bullet as conceptualized by the author.
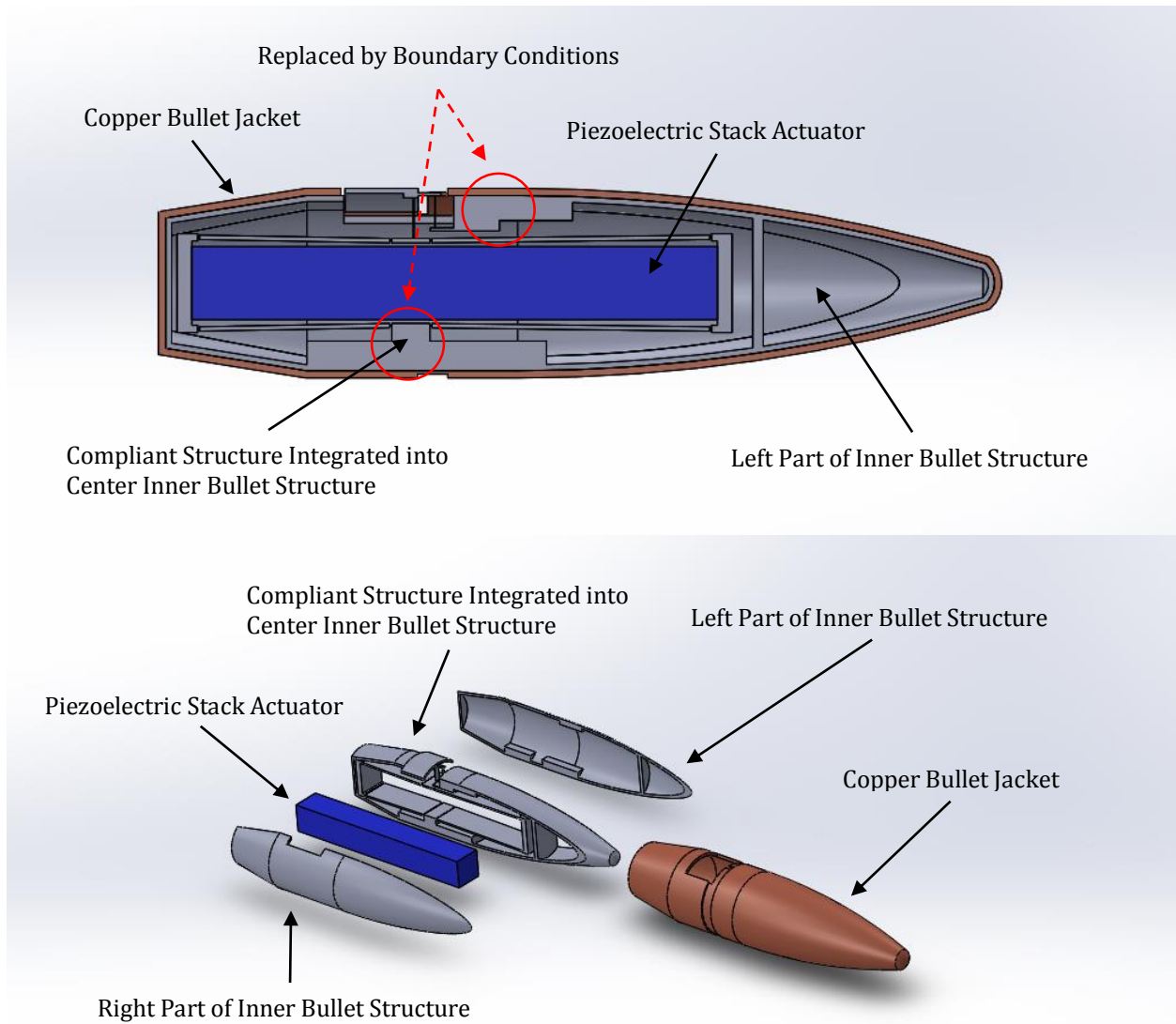
Replaced by Boundary Conditions

Copper Bullet Jacket

Piezoelectric Stack Actuator

Compliant Structure Integrated into
Center Inner Bullet Structure

Left Part of Inner Bullet Structure

Compliant Structure Integrated into
Center Inner Bullet Structure

Left Part of Inner Bullet Structure

Piezoelectric Stack Actuator

Copper Bullet Jacket

Right Part of Inner Bullet Structure

Figure 6: Conceptual smart bullet sans electronics and weights.

Top: Cross-sectional view. Bottom: Exploded view.

The above would require very precise machining. EDM or laser micromachining should be investigated. These manufacturing techniques may be costly, but given the rarity of using a smart bullet and the high-risk situations it may be used in, they should not be rejected. It should be noted that screw holes and screws were not modeled for simplicity, but they would be located at the thicker sections of the right, center, and left parts of the inner bullet structure. It should also be noted that most bullets are largely made of lead. The hollow nature of the smart bullet will affect flight and impact characteristics, and weights should be added to compensate.

Concluding Remarks

A solid-state smart actuator was designed for the purpose of engaging a spoiler on 0.50 caliber smart bullet. Although it does not undergo plastic deformation under the applied voltage and will survive a typical lifetime of a sniper bullet, the current design did not meet deployment requirements, reducing the possible total absolute change in flight trajectory. The lessons learned from the wind tunnel testing and structural finite element analysis can be applied for further verification and development. However, the methods and results are promising. The model can be further tuned to meet specifications, and a solid groundwork has been laid for future work done on the smart bullet project. Further work can now be done on multi-physics modeling, power, flight characteristics, impact characteristics, mass properties, configuration, tracking, and controls.

The author would like to direct attention to the Appendix, which offers other possible solutions to designing a smart bullet actuator.

Acknowledgments

I would like to thank my graduate and undergraduate predecessors in LIMS who have worked on the project and provided valuable information and results. The undergraduate students I worked with, Lisa Li and Christina Middleton, deserve my thanks. Lisa helped me explore multiple design options for the compliant structure simultaneously, saving a lot of time, and Christina helped make the presentation at the AIAA student conference more thorough with her help on the wind tunnel testing slides and effort in the actual testing. Both helped push the smart bullet project in the right direction.

Due to the reliance on ANSYS for this project, I would like to thank Dr. Rajesh Bhaskaran for his general assistance and helping me familiarize myself with ANSYS. Sean Harvey of ANSYS helped me with using the optimization tools and parameterization in ANSYS, which resulted in the project going more smoothly. David Roche of ANSYS created the Piezo extension and was a valuable support in the fall when there were some bugs in the extension, now resolved. Sean and David have my appreciation.

I would like to thank Boris Kogan for his help and work on the project. I primarily worked with him in the fall semester, and his approachability and advice in the past year have been greatly appreciated. Finally, I would especially like to give special thanks to Professor Garcia for his guidance and support. Professor Garcia and Boris welcomed me into LIMS as a new student (I did not attend Cornell for my undergraduate studies), they have my utmost gratitude.

References

Castelli, V. and Meng, Q., "A Design Method for Flexure-Based Compliant Mechanisms on the Basis of Stiffness and Stress Characteristics," Universita di Bologna, Bologna, Italy, 2012.

Chan. C, Li, L., and Middleton, C., "Smart Bullet Smart Actuator Design", Cornell University, April 2014 (unpublished AIAA student conference paper).

Howell, L., Magleby, S., and Olsen, B., *Handbook of Compliant Mechanisms*, 1st ed., John Wiley & Sons Ltd., United Kingdom, 2013.

Kogan, B. and Garcia, E., "Walking the Precession for Trajectory Control of Munitions," *Journal of Guidance, Controls, and Dynamics*, 2014 (in-press).

Leo, D., *Engineering Analysis of Smart Material Systems*, 1st ed., John Wiley & Sons, Inc., Hoboken, New Jersey, 2007.

Lobontiu, N. and Garcia, E., *Mechanics of Microelectromechanical Systems*, 1st ed., Kluwer Academic Publishers, New York, NY, 2005.

McCoy, R., "The Aerodynamic Characteristics of .50 Ball, M33, API, M8, and APIT, M20 Ammunition," Ballistic Research Laboratory, U.S. Army Laboratory Command, Jan. 1990.

Appendix

Personal Statement of Contribution

In the fall semester of 2013, I reported mainly to Boris Kogan, who had the general oversight and knew the progress of the project at that time. I also attended all lectures of Professor Garcia's MAE 6950 (Special Topics) course on smart materials to gain the background necessary to design smart actuators. I explored using Abaqus (prior to entering Cornell, I was proficient at Abaqus), COMSOL, and ANSYS for piezoelectric analysis, and chose ANSYS because it was widely used in LIMS and ANSYS Workbench was the easiest to use of the three. Choosing ANSYS would make future work more convenient. I familiarized myself with ANSYS and found ways to incorporate piezoelectric analysis into structural FEA, something that no one in LIMS had experience in. I explored using ANSYS Mechanical APDL and the recently released piezoelectric ACT extension for Workbench, Piezo, and found that using the extension in Workbench was easier, more efficient, and equivalent to using APDL. I also verified the Workbench results by looking at a mock scissor-jack actuator and verifying the extension's capabilities. The main conclusions from my investigations were that due to the elastic and piezoelectric properties of the stack actuator, applying displacements alone (replacing the stack actuator) to the compliant structure in ANSYS was not enough to provide results. Likewise, applying displacement signals for transient purposes were not sufficient as it did not accurately describe the behavior of the smart actuator. Lastly, my investigations found that the steel compliant structure's response (engagement and disengagement) to the stack actuator with a voltage signal was near instantaneous. These conclusions substantiated using ANSYS Workbench instead of APDL as a key tool for designing the smart actuator for LIMS's purposes, saving time for future students working on the project who have little or no prior experience using APDL.

During winter break, I researched on compliant mechanisms and drew potential topological designs for smart actuators that could be used for Gurney flap and spoiler deployment. I also realized that the previous model designed (I was not involved with the design) in the fall semester was incorrect, prompting full redesign in the spring semester.

In the spring semester of 2014, I took over the project since Boris departed from LIMS. I reported mainly to Professor Garcia and led the team, which consisted of Lisa Li, Christina Middleton, and me. Using the knowledge I had gained the previous semester, I took control of designing the compliant structure, and advised Lisa on engineering design and building intuition. I instructed her on which design options to explore. I also oversaw exchanges between Christina and the wind tunnel personnel at Syracuse University, as the wind tunnel testing had to be redone (still in progress at the time of this writing). Lastly, we presented our work at the AIAA Region-I Student Paper Conference at Cornell on April 25, 2014. I wrote most of the paper and created most of the presentation slides, which in total took two weeks of preparation. On a side note, I attended the on-campus ANSYS workshops in April to learn more about tools that could aid in designing the actuator.

Currently, all files related to the smart bullet project are being reorganized on the LIMS NAS server, and I am in the process of writing a short document describing the progress of the project so far. This is done so that should the project continue, people can be easily brought up to speed. Since I took MAE 6780 (Multivariable Control Theory) this spring, I am also working on a project that builds on Boris's work on smart bullet controls, utilizing a constrained Model Predictive Control with the Multi-Parameter Toolbox in MATLAB, hopefully providing an explicit control law that does not require online optimization. This project might also explore white noise disturbance (to simulate wind) rejection. All files regarding this project will be on the LIMS NAS server.

Finally, I am in the process of creating a tutorial for modeling piezoelectrics in ANSYS Workbench, which will be on Cornell Simcafe so that others can learn what I have learned.

It is my hope that I have laid the groundwork necessary to facilitate future work on the smart bullet project. Any question regarding the design of the smart actuator and this report can be emailed to ckc73@cornell.edu.

PIC255 Material Properties (Received from Physik Instrumente)

Material coefficients PIC255

Coefficent	Unit	Value	Coefficient	Unit	Value
Densitiy	kg/m³	7,80E+03	N1	Hzm	1420
Qm		80	N3	Hzm	1710
			N5	Hzm	1125
ε 11Tr		1649	Np	Hzm	2000
ε 33Tr		1750	Nt	Hzm	2000
ε 11Sr		930			
ε 33Sr		857	d31	m/V	-1,74E-10
			d33	m/V	3,94E-10
β 11T	Vm/As	6,85E+07	d15	m/V	5,35E-10
β 33T	Vm/As	6,45E+07			
β 11S	Vm/As	1,21E+08	g31	Vm/N	-1,13E-02
β 33S	Vm/As	1,32E+08	g33	Vm/N	2,54E-02
			g15	Vm/N	3,66E-02
tan δ		20,0E-3			
			e31	N/Vm	-7,15
k31		0,351	e33	N/Vm	13,70
k33		0,691	e15	N/Vm	11,90
k15		0,661			
kp		0,620	h31	N/As	-9,43E+08
kt		0,471	h33	N/As	1,81E+09
			h15	N/As	1,45E+09
Poisson (σ)		0,36			
s11E	m²/N	1,590E-11	c11E	N/m²	1,230E+11
s33E	m²/N	2,097E-11	c33E	N/m²	9,711E+10
s55E	m²/N	4,492E-11	c55E	N/m²	2,226E+10
s12E	m²/N	-5,699E-12	c12E	N/m²	7,670E+10
s13E	m²/N	-7,376E-12	c13E	N/m²	7,025E+10
s44E	m²/N	4,492E-11	c44E	N/m²	2,226E+10
s66E	m²/N	4,319E-11	c66E	N/m²	2,315E+10
s11D	m²/N	1,393E-11	c11D	N/m²	1,298E+11
s33D	m²/N	1,096E-11	c33D	N/m²	1,220E+11
s55D	m²/N	2,532E-11	c55D	N/m²	3,949E+10
s12D	m²/N	-7,660E-12	c12D	N/m²	8,345E+10
s13D	m²/N	-2,945E-12	c13D	N/m²	5,729E+10
s44D	m²/N	2,532E-11	c44D	N/m²	3,949E+10
s66D	m²/N	4,319E-11	c66D	N/m²	2,315E+10

Values are only for information - no specification!
Simulation purpose

The data in the table was determined using test bodies with geometries and dimensions in accordance with European Standard EN 50324 2, and are typical values.

Singular parameters can deviate from catalogue values, because they were measured at samples which were taken from one block of ceramics according to the sequence of IEC483 to get maximum consistency.
Catalogue values reflect the statistical distribution of each individual specification in production and therefore also take into account spreading from material batch to material batch.

Fall Semester Investigations

A summary of my investigations in the fall can be found in the "Statement of Personal Contribution" section above.

The below table shows the equivalent conversions for modeling piezoelectric stacks in ANSYS. This was obtained from the official blog of ANSYS (http://www.ansys-blog.com/multilayer-piezoelectric-actuators-can-single-layer-modeled-simulate-layered-stack/).

		Single Layer	Multi-layer Stack	Bulk	Ratio (Bulk/multi-layer)
Input	Voltage	$V_s = \dfrac{V_b}{n}$	$V_M = \dfrac{V_b}{n}$	$V_b = n.V_s$	n
Output quantities	Electric Field	$E_s = \dfrac{V_s}{th}$	$E_M = \dfrac{V_M}{th}$	$E_b = \dfrac{V_b}{L_h} = \dfrac{V_b}{n\times th}$	1
	Strain	$\varepsilon_s = d.E_s$	$\varepsilon_M = d.E_M$	$\varepsilon_b = d.E_b$	1
	Stroke	$\Delta L = th.\varepsilon_s = th.d.E_s$	$\Delta L = n.th.\varepsilon_M = n.th.d.E_M$	$\Delta L = th.\varepsilon_d = n.th.d.E_d$	n
	Electric Flux Density	$D_s = \kappa.E_s$	$D_M = \kappa.E_M$	$D_b = \kappa E_b$	1
	Electric Charge Q	$Q_s = n.D_s.A = \kappa.E_s.A$	$Q_M = n.D_M.A = n.\kappa.E_M.A$	$Q_b = D_b.A = \kappa.E_b.A$	$\dfrac{Q_b}{Q_s} = \dfrac{1}{n}$
	Capacitance C	$C_s = \dfrac{\kappa.A}{th}$	$C_s = n.\dfrac{\kappa.A}{th}$	$C_b = \dfrac{\kappa.A}{L_h} = \dfrac{\kappa.A}{n.th}$	$\dfrac{C_b}{C_s} = \dfrac{1}{n^2}$

Calculations were done to compare ANSYS results for the piezoelectric stack. For a stack:

$$\delta_0 = \frac{d_{33}L_3}{t}V$$

$$f_{bl} = \frac{d_{33}A}{s_{33}^E t_p}V$$

Given:
V_{layer} = 120 V, A = 5 mm x 5 mm, L_3 = 36 mm, t_p = 0.05 mm
d_{33} = 3.94E-10 m/V

Calculated:
$n = \frac{L_3}{t} \to V_{bulk} = V_{layer} * n = 72000\,V$
$s_{33}^E = d_{33}\,E_3, E_3 = \frac{V_{layer}}{L_3} = 3333.33\,V/m$

Piezoelectric stack static modeling (units in figure below are in mm):
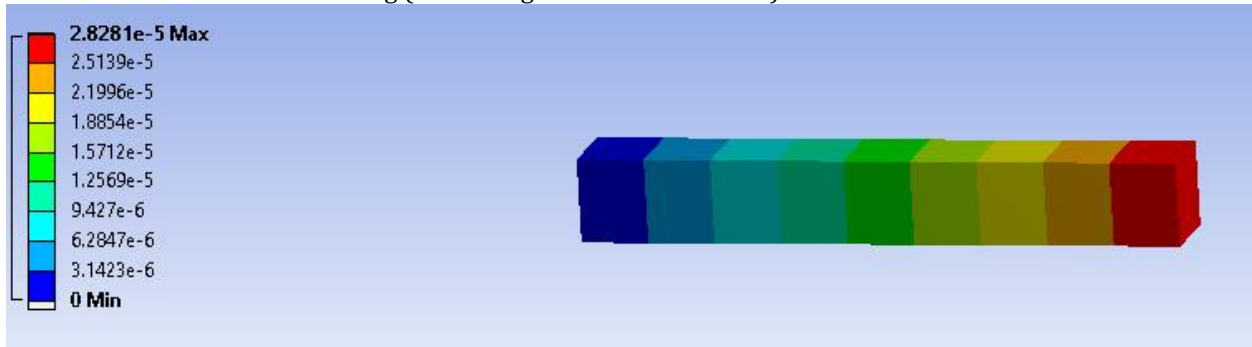
Results:

	Given	Calculated	ANSYS	ANSYS Error from Calc.	ANSYS Error from Given
Free disp. (μm)	38 ± 10%	34.04	28.281	-16.9%	-25.6%
Blocked force (N)	950	1127.32	936.52	-16.9%	-1.4%

The following can be done to adjust the model:
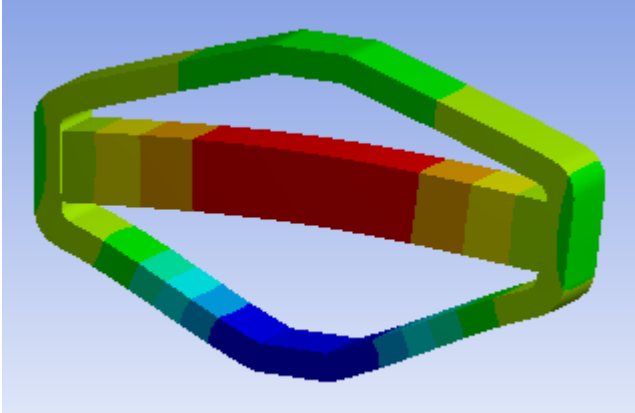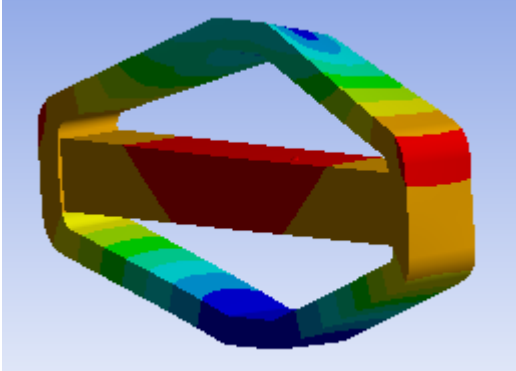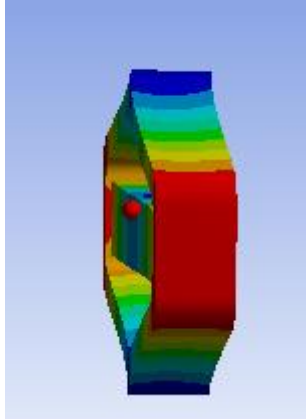
$e = Y^E d$ is used for ANSYS input. $Y_{33}^E = \frac{1}{s_{33}^E}$ (or Young's modulus in the 3-3 direction) should be increased for new ANSYS input, as increasing voltage will not adjust for both blocked force and free displacement accordingly. d_{33} can then be changed using the blocked force equation. This can be an iterative process to provide a more accurate model if desired.
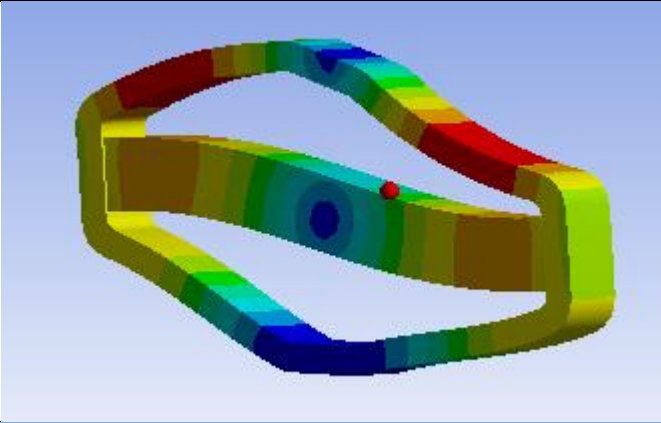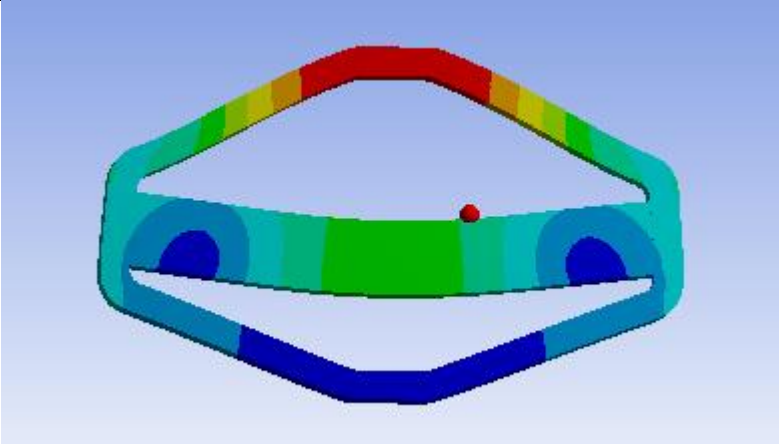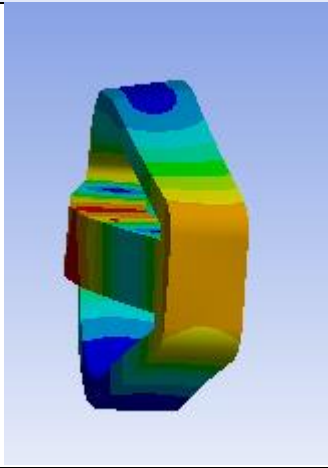
Example Mock Scissor Jack Actuator:
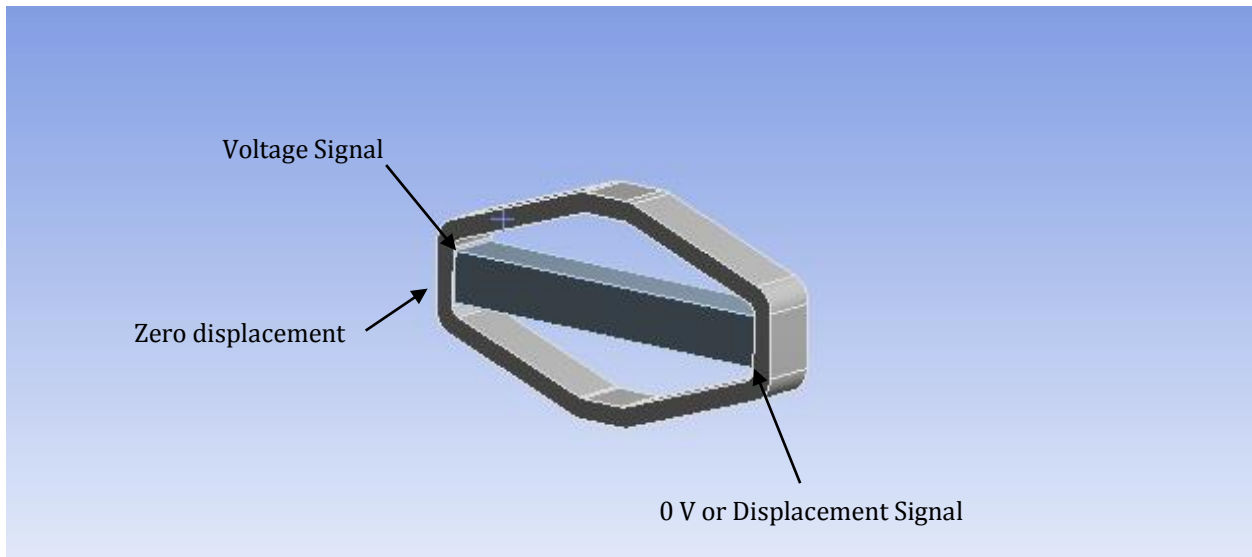
Modal Analysis

The table below demonstrates modal analysis while using the Piezo extension. Due to time constraints, this was not done for the actual actuator discussed in the technical report above.

Frequency (Hz) without piezo properties	Frequency (Hz) with piezo properties	Mode
1625.7	1652.3	
1815.5	1830.8	
5868.5	5875.8	

7838.4	7980.8	
9310.7	9587.3	
10245	10601	

The differences in the two sets of frequencies showed that the piezoelectric properties could not be ignored in modal analyses.

Transient Analysis (displacement function and voltage signal)

This analysis was done to compare using a displacement signal versus a voltage signal.

At 2500 Hz,

$$V(t) = \frac{72000 Volts}{2} \sin\left(2500 \cdot 2\pi t - \frac{\pi}{2}\right) + \frac{72000 Volts}{2}$$

$$x(t) = \frac{38\,\mu m}{2} \sin\left(2500 \cdot 2\pi t - \frac{\pi}{2}\right) + \frac{38\,\mu m}{2}$$

This gave the following plot:
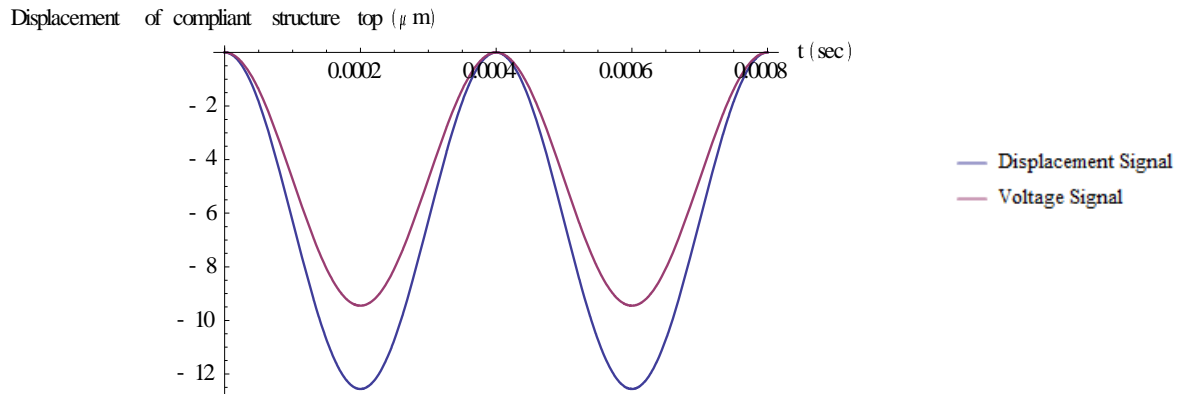
As can be seen above, using a voltage signal results in a more conservative model. This is also more realistic because the piezoelectric stack has elastic properties that must be taken into account.

Miscellaneous information about the mock scissor-jack actuator above using piezoelectric static structural analysis were as follows:

Max horizontal displacement: 8.21 μm
Max vertical displacement: -9.45 μm
Amplification: 1.15 x

Likewise, transient analysis was not explicitly done with the actuator discussed in the technical report due to time constraints.

Attempted Iterations and Comments

It is my hope that this section helps provide a "lessons learned" account on designing the compliant structure. This and the technical report should give the full picture.

The first three iterations all utilized small-pivot flexures except for the link connecting the spoiler to the bullet structure. The first attempt (shown below) was ultimately used for the AIAA student conference. This iteration was given two months in the spring semester to complete. Many adjustments were done to the model to test its potential.
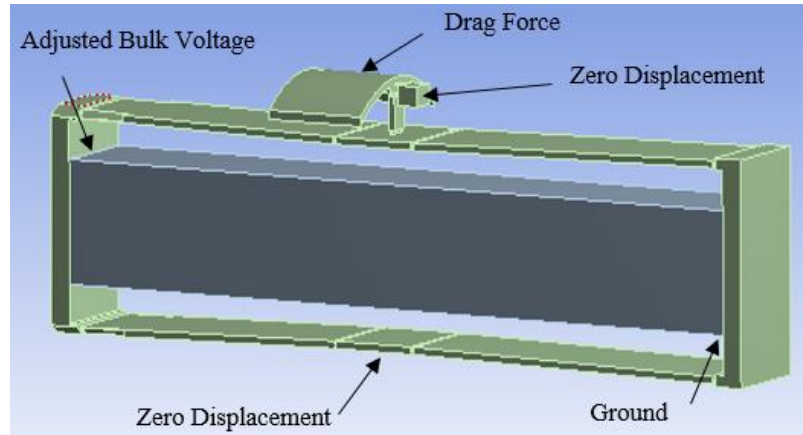
The bow-tie structure alone had the same vertical displacement as the current design, and simple geometric calculations given a kinematic structure predicted that a 2 mm deployment would be reached. However, this was not the case. It reached 0.67 mm vertical spoiler displacement and had a maximum von-Mises stress of 1133 MPa. Upon closer inspection of the upper amplification structure (below), the problem was clear.
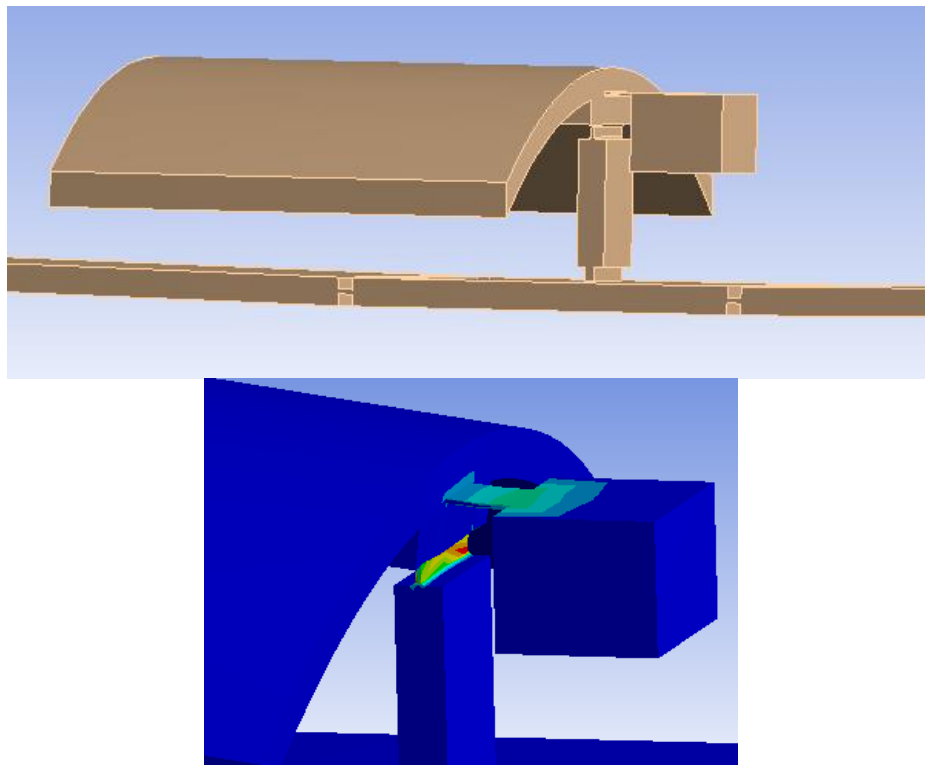
Due to the very short length of the flexure in the lever arm, in which both ends used the small-length flexural pivot, there was a high torsional stiffness, this resulted in the high stress concentrations (shown in red above). It was also observed that the link connecting the spoiler to the simulated inner bullet structure (shown as a cube-like structure above) was very compliant and long. This resulted in less of a mechanical advantage from the lever arm to the spoiler and more resistance against angular rotation of the spoiler. Instead, the flap mainly translated vertically. However, these conclusions were reached after the second and third attempts were done. I would advise that using small-length flexural pivots for a lone lever arm connecting the bow-tie structure to the spoiler should be avoided unless an alternate upper amplification structure is found to be successful. The advantage of using the small-length flexural pivots is the resistance to disturbances or large aerodynamic forces, and the disadvantage, again, is the high stress concentrations.

The second attempt, given a week to explore and was done two weeks before the AIAA student conference, utilized the following ball and stick model:
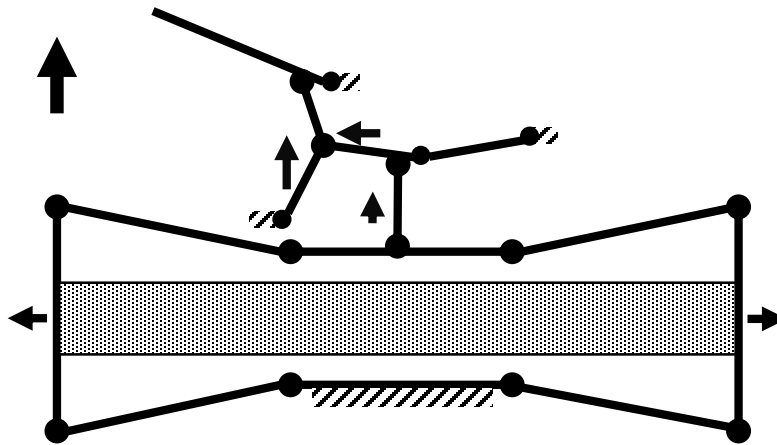

The idea for this was obtained from the *Handbook of Compliant Mechanisms*, shown below:
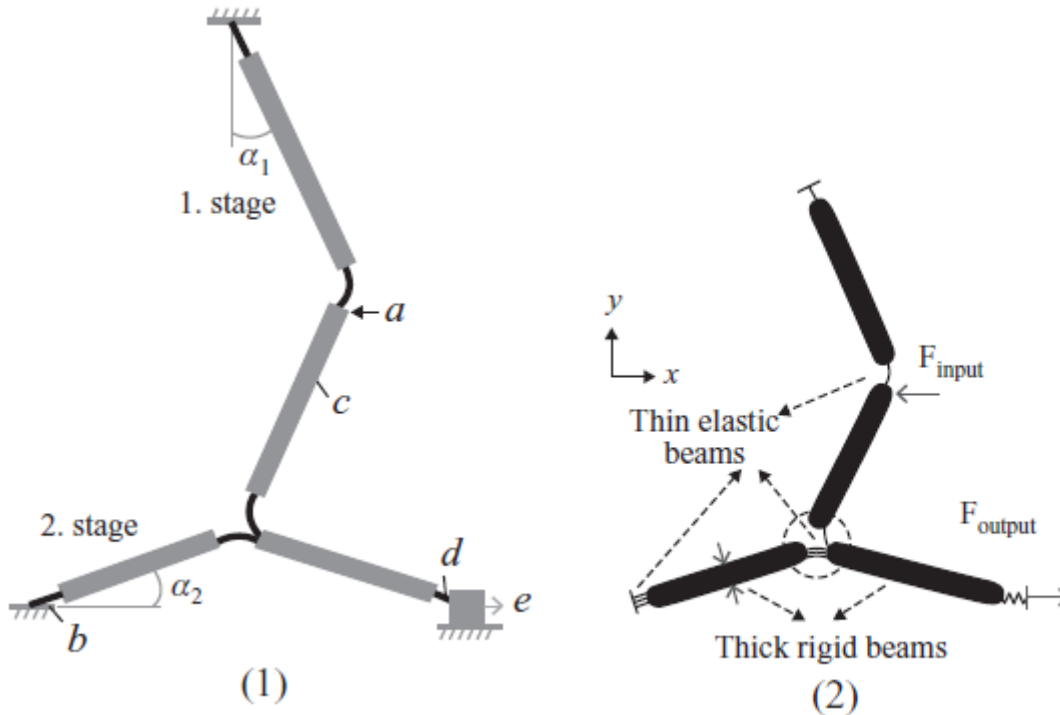
Due to time constraints, this model was not fully explored, but reached similar numbers to the first attempt. I recommend that more investigations be done on this as the overall greater torsional stiffness will have a stronger actuator, and with the right dimensions, should reduce stress concentrations.

The third attempt used a double-lever system, which looked like a double-flap system. As a kinematic structure, this should have provided the greatest amplification ratio of all attempts. This was explored the week before the AIAA student conference.
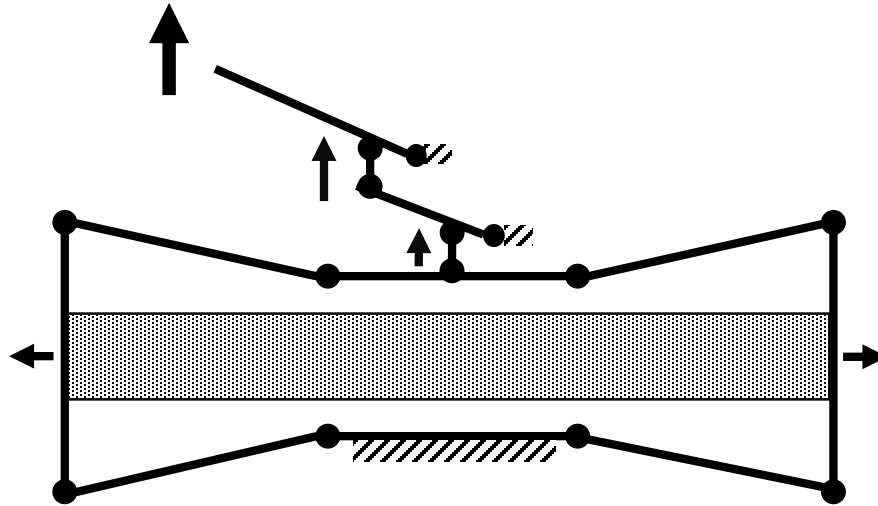
The results were worse than the second iteration. However, given the new upper amplification system of the current design, this should be explored again in the future. It is important to note that the torsional stiffness of the lower half of the upper amplification system should be greater than that of the upper half, yet less than the torsional stiffness of the bow-tie structure in order to maximize amplification.

The current model uses the following upper amplification structure:
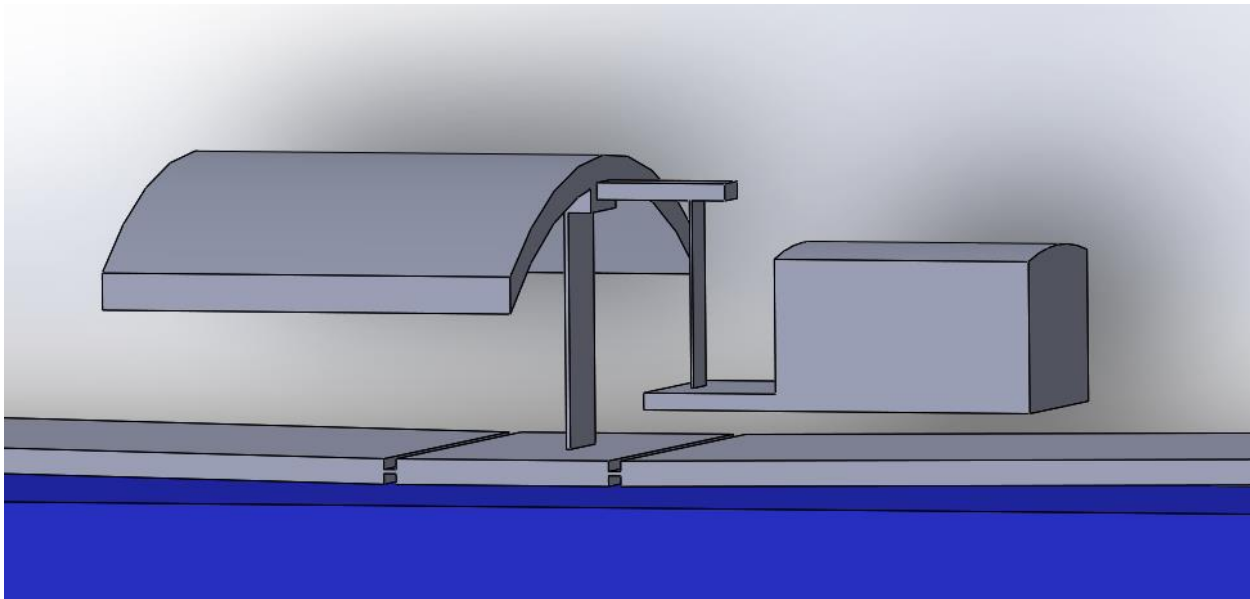
Using the lessons learned above, the current greater deployment and lesser maximum von-Mises stress were reached. This allowed greater rotation of the spoiler while reducing stress concentrations.

Additional Compliant Mechanism Plans, Solutions

The following scan shows other possible ball and stick models with advantages and disadvantages of each. These were done before anything was modeled in SolidWorks and ANSYS. These sketches allowed for both Gurney flap and spoiler deployment. However, it should be noted that any dual deployment system should deploy and retract 90° apart from each other about the spin axis of the bullet as well as oscillate 180° out of phase with each other.
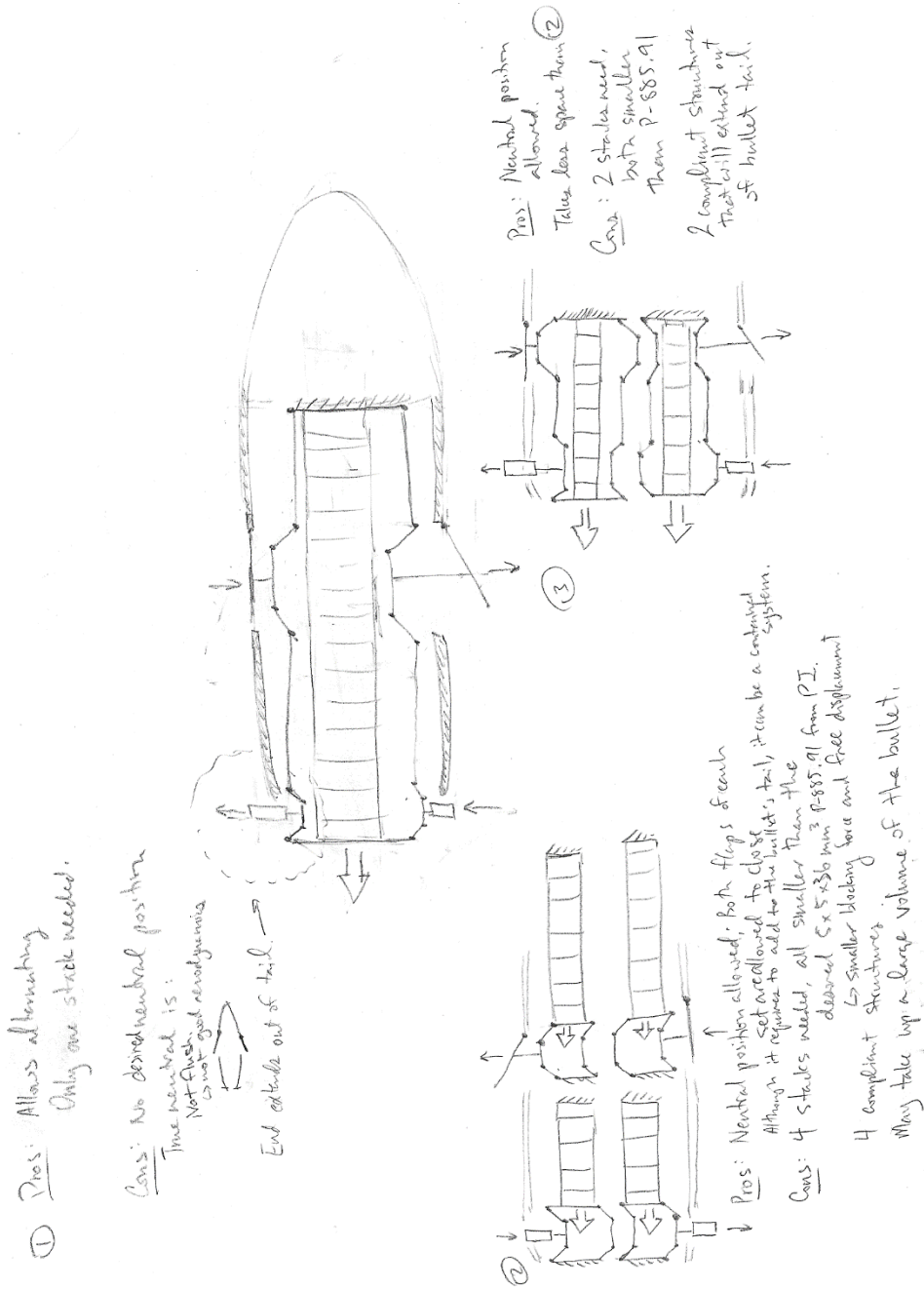
Should there be insufficient room in the smart bullet for other components, an octagon lower amplification structure with a smaller piezoelectric stack (such as a 5 mm x 5 mm x 18 mm stack) rather than a bow-tie structure should be investigated. Utilizing the above methods and learned lessons should facilitate the design process. This will also result in a simpler design because symmetry may be used. Below shows the ball and stick model for such a design:
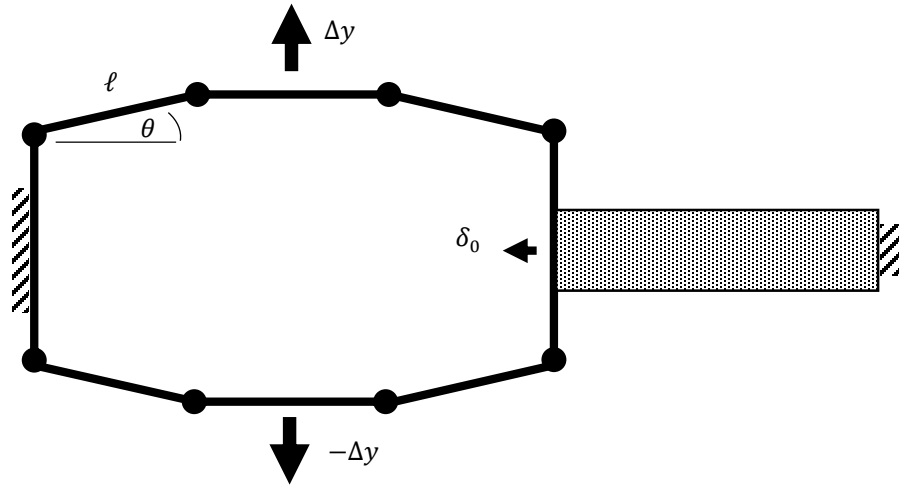

Using the same notation as the technical report, the equations describing the kinematic structure are

$$\delta_0 = \ell(\cos\theta - \cos\theta')$$
$$\Delta y = \ell(\sin\theta' - \sin\theta)$$

Note that once again, the top and bottom center links do not contribute to the above equations. The above results in an optimal angle of

$$\theta_{opt} = \cos^{-1}\frac{\delta_0}{2\ell}$$

Should the preliminary CFD analysis and current actuator design not practically work due to larger aerodynamic forces than expected, then a hybrid actuator should be considered. This hybrid actuator should utilize a primary compliant structure to amplify the piezoelectric stack actuator, but utilize hinges to deploy the spoiler. It should be noted that this no longer becomes a fully solid-state actuator. For example, the hinges can be located at the top of the compliant structure (if using a bow-tie or octagon), the bottom of the spoiler (near the front), and at the front face of the spoiler connecting the spoiler to the rest of the bullet. A connecting arm can connect the hinge at the top of the compliant structure to the hinge at the bottom of the spoiler. This should allow for a larger torsional stiffness to be designed in the compliant structure, resulting in a stronger actuator. The elastic properties of the compliant structure, aided by aerodynamic forces, will restore the spoiler to a disengaged position. The figure below demonstrates this example:
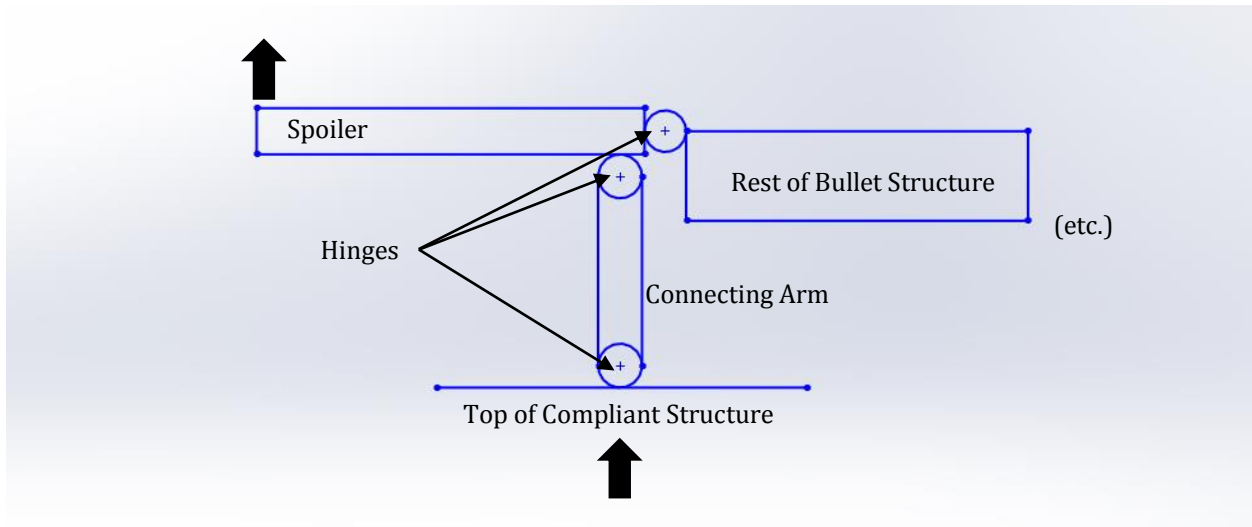
Should a more capable piezoelectric actuator be needed, a single-crystal piezoelectric actuator can be considered. Single-crystal actuators can withstand higher voltages than stack actuators, and this results in higher deflections. Estimates from TRS Technologies give the following information on their single-crystal piezoelectric actuators:

Description	Approximate Maximum Voltage	Estimated Maximum Stroke (μm)	Estimated Price
5x5x36 mm^3, 0.5 mm plates	500 V	>> 35 μm	$3,640
5x5x18 mm^3, 0.257 mm plates	260 V	>> 16 μm	$3,400
5x5x18 mm^3, 0.5 mm plates	500 V	>> 18 μm	$2,510

TRS stated that the strokes were estimates. Theoretically, they would be even larger. However, since the actuators are clamped and the performance is reduced due to the stacking of the layers and the epoxy, the exact impact was difficult to calculate. Their PMNT29 material has the following properties:

MEASURED AND DERIVED ELASTIC COMPLIANCE CONSTANTS, s_{ij} (10^{-12} m²/N), AND ELASTIC STIFFNESS CONSTANTS, c_{ij} (10^{10} N/m²), FOR PMNT29

Material	s_{11}^E	s_{12}^E	s_{13}^E	s_{33}^E	s_{44}^E	s_{66}^E	s_{11}^D	s_{12}^D	s_{13}^D	s_{33}^D	s_{44}^D	s_{66}^D
PMNT29	52.1	-24.6	-26.4	59.9	16.0	28.3	41.8	-34.8	-3.9	10.3	14.0	28.3

Material	c_{11}^E	c_{12}^E	c_{13}^E	c_{33}^E	c_{44}^E	c_{66}^E	c_{11}^D	c_{12}^D	c_{13}^D	c_{33}^D	c_{44}^D	c_{66}^D
PMNT29	12.4	11.1	10.4	10.8	6.3	3.5	12.6	11.3	9.3	16.8	7.1	3.5

TABLE II. Piezoelectric Coefficients, d_{ij} (pC/N), e_{ij} (C/m²), g_{ij} (10^{-3}Vm/N), h_{ij} (10^8V/m), and Electromechanical Coupling Factors, k_{ij}, For PMNT29

Material	d_{33}	d_{31}	d_{15}	e_{33}	e_{31}	e_{15}
PMNT29	1540	-699	164	22.3	-3.9	10.3

Material	g_{33}	g_{31}	g_{15}	h_{33}	h_{31}	h_{15}
PMNT29	32.2	-14.6	11.9	27.7	-4.8	8.7

Material	k_{33}	k_{31}	k_{15}	k_t	k_{31} (45°C)
PMNT29	0.91	0.44	0.35	0.60	0.81

Dielectric Constants, ε_{ij} (e_0), and Dielectric Impermeability Constants, β (10^{-4}/e_0), For PMNT29

Material	ε_{33}^T	ε_{11}^T	ε_{33}^S	ε_{11}^S	β_{33}^T	β_{11}^T	β_{33}^S	β_{11}^S
PMNT29	5400	1560	910	1340	1.85	6.41	10.99	7.46

* Ec: 1.8-3kv/cm, Trt: 80-100°C

The people to contact at TRS Technologies would be Jenna VanLeeuwen (jenna@trstechnologies.com) or Raffi Sahul (raffi@trstechnologies.com). Refer to the project as the "Cornell smart actuator project" when communicating with them.

# ANSYS Workbench Piezoelectric Tutorial

This ANSYS tutorial provides the steps needed for a quasi-static structural analysis of the actuator discussed in this report. The files needed can be found on the LIMS NAS server. This tutorial assumes some familiarity with ANSYS Workbench and that the piezoceramic PIC255 from PI is used.

1. Download the Piezo extension for ANSYS 14.5 or 15 from the ACT Extension Library of the Customer Portal (https://support.ansys.com/AnsysCustomerPortal/en_us/Downloads/Extension+Library/ACT+Library).
2. Install from the Workbench Project page.
   a. Select "Extensions" -> "Install Extension"
   b. Select the *.wbex file when the file explorer window opens.
3. Open the project file "SB_Actuator.wbpj".
4. Under material properties, check that material PIC255 is there with the following material properties (which can be found on the PIC255 datasheet above). If not, add it to the library.

	A	B	C	D	E	F
1	(Pa)	(Pa)	(Pa)	(Pa)	(Pa)	(Pa)
2	1.23E+11					
3	7.67E+10	1.23E+11				
4	7.025E+10	7.025E+10	9.711E+10			
5	0	0	0	2.226E+10	7780	
6	0	0	0	0	2.226E+10	
7	0	0	0	0	0	2.315E+10

The density of PIC255 should be set to 7800 kg/m^3.

5. Part of the workspace should have the following modules:
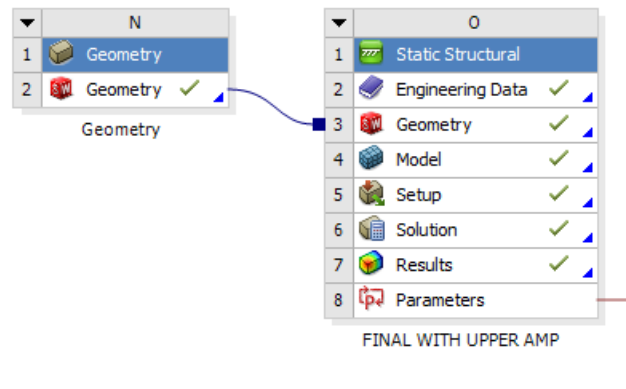
The module on the right is a renamed Static Structural module. If the assembly file is open in SolidWorks, the geometry can be updated by right-clicking the "Geometry" box on the left with the SolidWorks icon and selecting Update from CAD. Note that there is a "Parameters" box. Any SolidWorks dimension labeled with "DS_" as a prefix will show up as a parameter in ANSYS which can be adjusted or optimized. For a tutorial on using the optimization tool, see the "Plate with a Hole: Optimization" example on the Cornell ANSYS Simcafe website.

6. After clicking on the "Model" box. On the left, you should be able to see the following (or some variant of it):
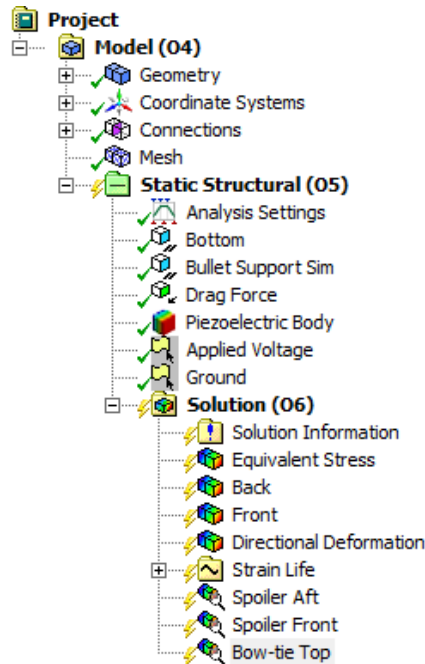
7. Go to the Analysis Settings and ensure that the following is set:

There are 2 steps for allowing the actuator to fully engage and then applying the drag force. It is important that the Solver Type is "Direct" to allow for very small deflection modeling. Setting it to anything else will cause the model to fail.

8. Select "Piezoelectric Body" and check that the following is set:
Notice that the polarization axis is in the Z direction. Make sure that the actuator poling direction (or bullet's spin axis) is aligned along the Z direction. If not, the results will be inaccurate. Select the piezoelectric stack as the designated body.

Details of "Piezoelectric Body"

Scope	
Scoping Method	Geometry Selection
Geometry	1 Body
Definition	
Polarization Axis	Z
Permittivity Constant	8.854E-12 [A A sec sec sec sec kg^-1 m^-1 m^-1 m^-1]
PIEZ e31	-7.15 [A sec m^-1 m^-1]
PIEZ e33	13.7 [A sec m^-1 m^-1]
PIEZ e15	14.46 [A sec m^-1 m^-1]
DPER ep11	1650
DPER ep33	1750
RSVX	0 [kg m m m A^-1 A^-1 sec^-1 sec^-1 sec^-1]
RSVY	0 [kg m m m A^-1 A^-1 sec^-1 sec^-1 sec^-1]
RSVZ	0 [kg m m m A^-1 A^-1 sec^-1 sec^-1 sec^-1]
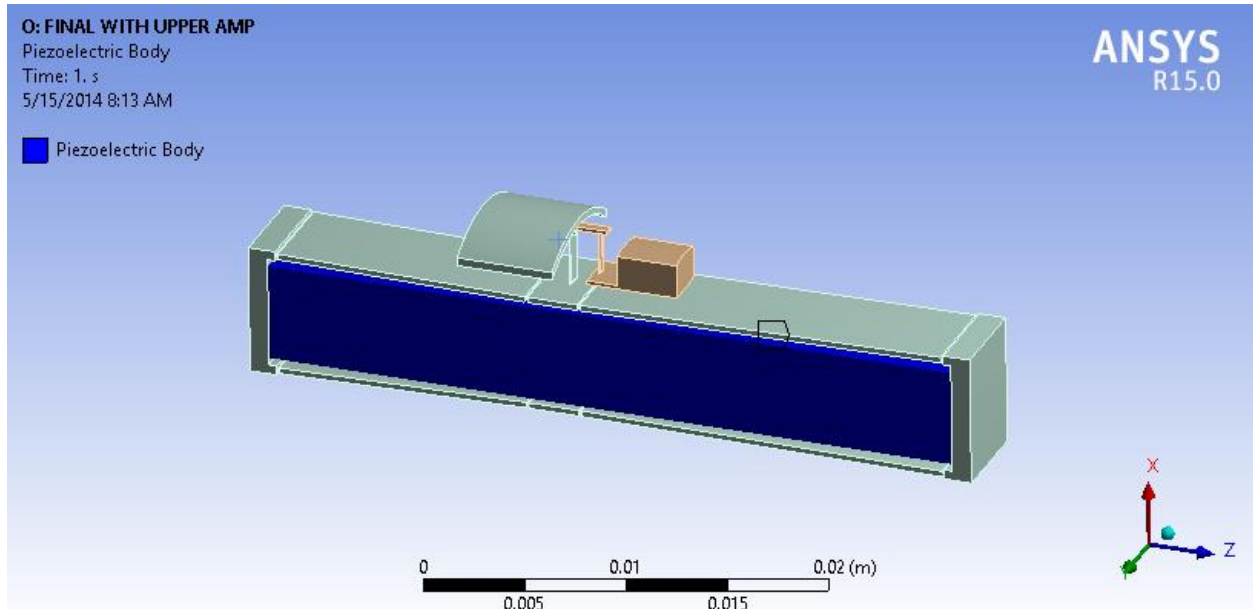
9. Going down the list of boundary conditions, ensure that the following is set and/or selected:
   a. Bottom
   Note that zero-displacement boundary conditions are used instead of fixed support. Using fixed supports as boundary conditions in ANSYS will cause the Piezo extension to malfunction.

   b. Bullet Support Sim

c. Drag Force
Note that the -2.67 N is from the CFD preliminary analysis.

Details of "Drag Force"		卓
Scope		
Scoping Method	Geometry Selection	
Geometry	1 Face	
Definition		
Type	Force	
Define By	Components	
Coordinate System	Global Coordinate System	
☐ X Component	0. N (ramped)	
☐ Y Component	0. N (ramped)	
Z Component	Tabular Data	
Suppressed	No	

Tabular Data

	Steps	Time [s]	☑ X [N]	☑ Y [N]	☑ Z [N]
1	1	0.	0.	0.	0.
2	1	1.	0.	0.	0.
3	2	2.	= 0.	= 0.	-2.67
*					

O: FINAL WITH UPPER AMP
Drag Force
Time: 1. s
5/15/2014 8:19 AM

Drag Force: 0. N
Components: 0.,0.,0. N

ANSYS
R15.0

0   0.005   0.01 (m)
  0.0025   0.0075
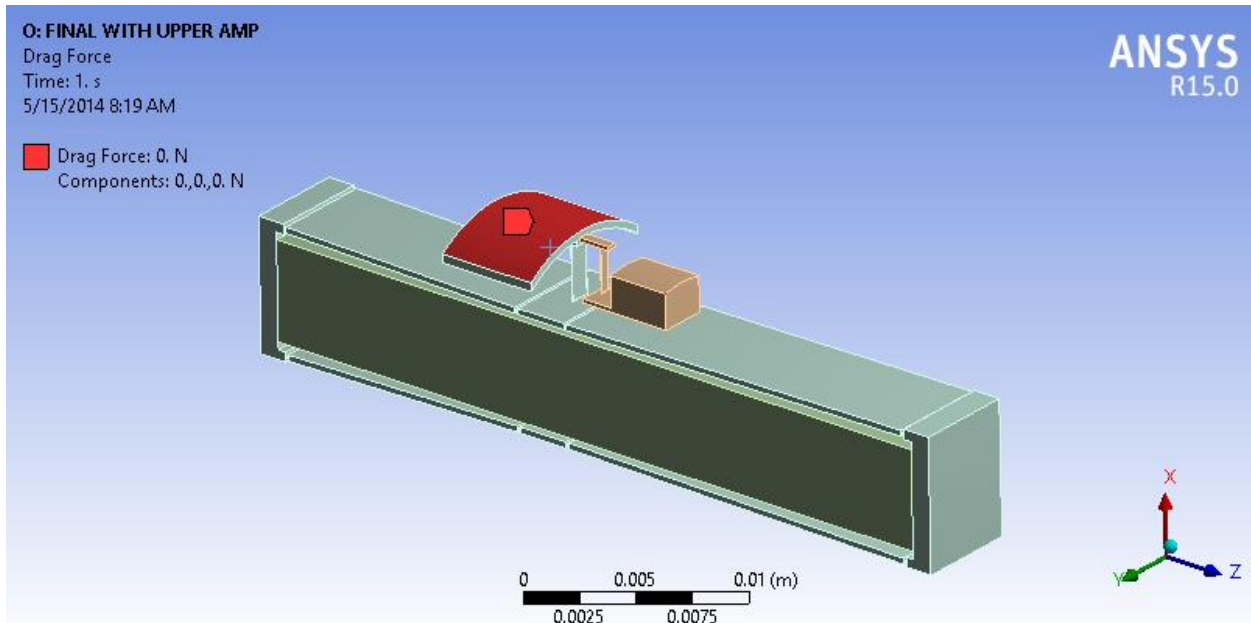
d. Applied Voltage
    Note that this is the adjusted bulk voltage. Make sure that the stack face is selected, not the larger face of the compliant structure that is in direct contact with it.
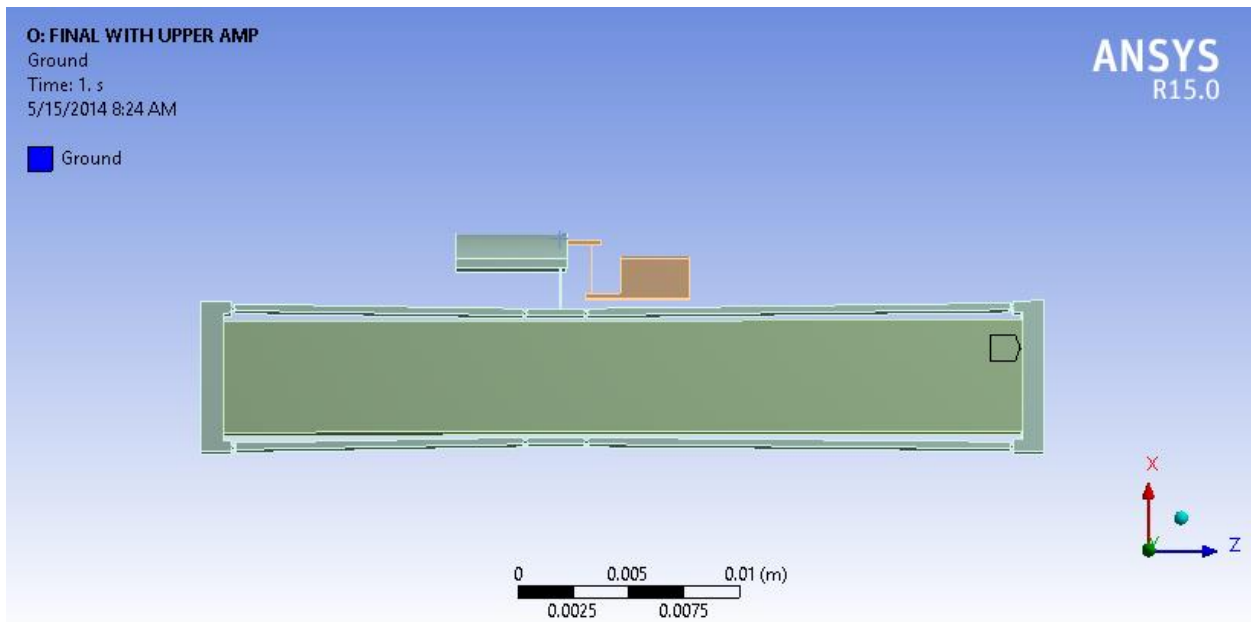
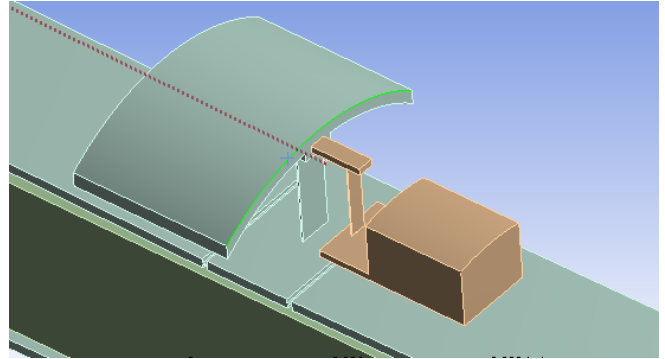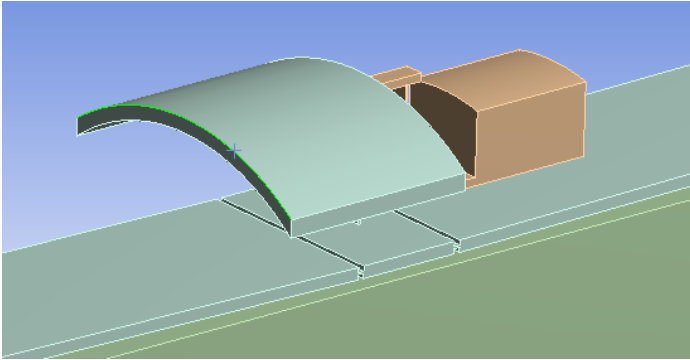| Details of "Applied Voltage"		⏻
□ **Scope**		
Scoping Method	Geometry Selection	
Geometry	1 Face	
□ **Definition**		
Time Dependency	No	
Voltage (Real)	17500 [kg m m A^-1 sec^-1 sec^-1 sec^-1]	
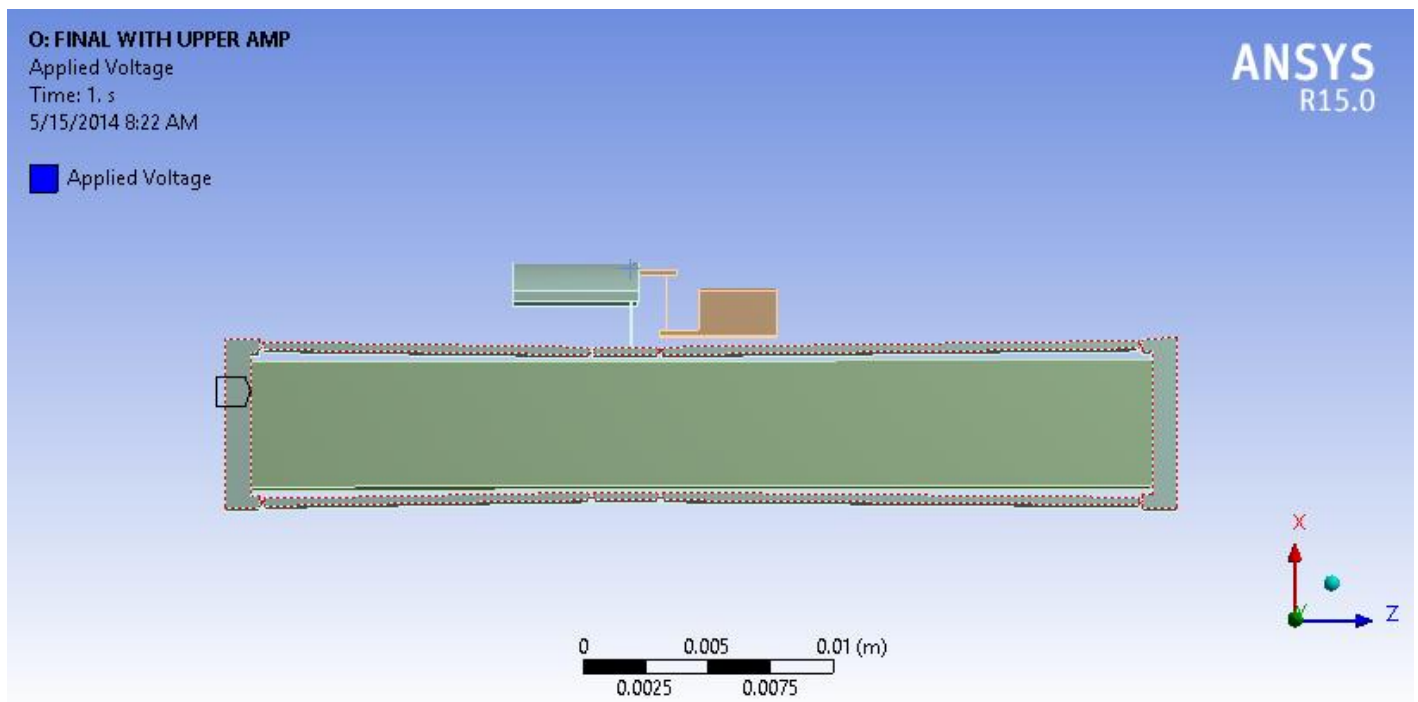
e. Ground

This is very similar to the applied voltage boundary condition. If the simulation gives a nonsensical behavior, specifically if the actuator acts in the opposite direction, switch the locations of the Applied Voltage and Ground boundary conditions.

Details of "Ground"		卫
⊟ **Scope**		
Scoping Method	Geometry Selection	
Geometry	1 Face	
⊟ **Definition**		
Time Dependency	No	
Voltage (Real)	0 [kg m m A^-1 sec^-1 sec^-1 sec^-1]	

O: FINAL WITH UPPER AMP
Ground
Time: 1. s
5/15/2014 8:24 AM

ANSYS
R15.0

■ Ground

0	0.005	0.01 (m)
	0.0025	0.0075

X
Z

10. Under the Solution section, Equivalent Stress should be selected for only the compliant structure (although all bodies are accepted), Back should have the same face selected as Applied Voltage, and Front should have the same face selected as Ground.
11. Directional Deformation should have an X-axis orientation. All bodies are accepted.

12. Spoiler Aft and Spoiler Front should be selected as such as the top back edge of the spoiler (shown below, left) and the top front edge of the spoiler (shown below, right), respectively. The edges are highlighted in green. The lower the front displacement, the more aerodynamic the spoiler is.

Use the same settings for both:

13. Bow-tie Top should have the top face of the compliant structure selected, and like before, the X-axis should be selected as the orientation.
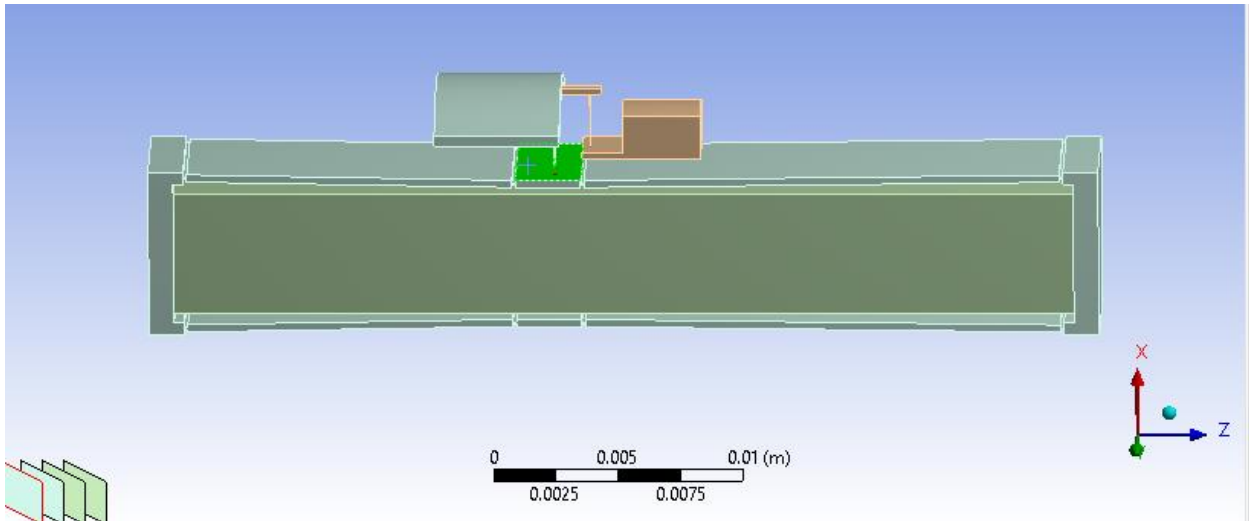
14. If Strain Life (or "Fatigue Tool") does not show under Solution, right click Solution, then click Insert -> "Fatigue" -> "Fatigue Tool". Click Strain Life (or "Fatigue Tool") and make sure that "Strain Life" is selected for the analysis type. Strain Life can be used for low and high cycles, whereas Stress Life is used for mainly high cycles. Make sure the piezoelectric stack is not selected as one of the bodies for "Life" and "Safety Factor." Similarly, these can be selected as solutions if Strain Life (or "Fatigue Tool") is right clicked. Then, select Insert -> "Life" or "Safety Factor." Ensure that the following setting for Strain Life (or "Fatigue Tool") is used:

Materials	
Fatigue Strength Factor (Kf)	1.
Loading	
Type	Fully Reversed
☐ Scale Factor	1.
Definition	
☐ Display Time	End Time
Options	
Analysis Type	Strain Life
Mean Stress Theory	SWT
Stress Component	Equivalent (Von Mises)
Infinite Life	1.e+009 cycles
Life Units	
Units Name	cycles
1 cycle is equal to	1. cycles

15. Ensure that the mesh is fine enough. Refinements may need to be done at the flexure edges. The thicker parts are rigid enough; the mesh does not have to be fine there.
16. Click Solve.
17. Observe results under "Solution."